doi.org/10.52568/001874/JCSP/48.02.2026

Modified Preparation of $TiO_2/BaSO_4$ Composite and Its Effects on PVC: Photodegradation, Flame-retardant and Mechanical Properties

Qiang Yang, Wei Gong, Chunsheng Zhou, Xiaowei Cui*

[1]*College of Chemical Engineering and Modern Materials, Shaanxi Key Laboratory of Comprehensive Utilization of Tailings Resources, Shangluo University, Shangluo 726000, Shaanxi Province, P.R. China*.

yq_sust@163.com*

(Received on 3rd February 2025, accepted in revised form 8th December 2025)

Summary: This study demonstrates a streamlined sol-gel strategy for synthesizing TiO_2 modified $BaSO_4$ composite particles, aiming to enhance the UV resistance, flame-retardant, and mechanical properties of PVC. The composite was systematically characterized using FT-IR, XRD, SEM, and laser particle size analysis. Results revealed that a TiO_2 molar ratio (n_{Ti}) of 2.0 mol yielded the most uniform particle size distribution (256-713 nm), along with a maximum settling time of 28.5 h and an activation degree of 82.8 %, which represented increases of 26.0 h and 49.5 %, respectively, over unmodified $BaSO_4$. When incorporated into PVC at 15 wt%, the composite significantly improved material performance: the limiting oxygen index (LOI) reached 27.6 %, Rhodamine B (RhB) photodegradation efficiency attained 70.2 %, and peel strength increased to 151.52 $N \cdot mm^{-1}$, exceeding unmodified PVC by 23.36 $N \cdot mm^{-1}$. Moreover, after 150 h of UV aging, the composite reinforced PVC retained superior mechanical integrity, with only 18.64 % loss in tensile strength and 10.32 % in peel strength. These findings confirm that the $TiO_2/BaSO_4$/PVC composite developed here offers a promising combination of enhanced durability and flame-retardant performance.

Keywords: $BaSO_4$; PVC; Sol-gel method; Mechanical properties; UV resistance.

Introduction

PVC was commonly used in building materials, electrical power cables, and process packaging due to its simple preparation process, long service life, and good mechanical properties. [1] During the process of forming PVC polymers, the molecular chain structure generated by free radical polymerization was not regular, and there were certain structural defects, resulting in poor flame-retardant performance and comprehensive mechanical properties. [2, 3]

Barite was a joint mineral in China, and its purified form, Barium sulfate ($BaSO_4$), was frequently used as an inorganic filler in the plastics, paper, coatings, and rubber industries. This filler had several advantages, including enhancing the optical properties and flame-retardant property of the substrate, increasing mechanical strength, and reducing production costs. During the drying stage, $BaSO_4$ filler particles had a tendency to agglomerate, leading to reduced dispersion and limiting the comprehensive utilization of the composite material. [4] To address this issue, $BaSO_4$ modified particles have been developed using coupling agents, [5] surfactants, [6] composite modifiers, [7] and inorganic materials. [8] For instance, Yang *et al* [9] prepared stearic acid modified PLA/$BaSO_4$ composites. The results demonstrated that the highest impact toughness and breaking elongation of the composites were generated when the mass fraction of $BaSO_4$ was 15%. The experiments additionally revealed that the effect of $BaSO_4$ on the thermal behavior of PLA was not significant, but the thermal stability of the composites was improved at high temperatures. The surface deposition layer of modified $BaSO_4$ particles effectively weakened the cohesive energy, prevented the agglomeration of $BaSO_4$ particles, making the modified $BaSO_4$ particles had a uniform particle size distribution, so as to improve the dispersion in the composite substrate. [10, 11]

TiO_2 had excellent surface properties. The combination of TiO_2 and inorganic materials improves the problems of easy agglomeration of inorganic substrates, poor dispersion, and recycling difficulties. Additionally, it enhanced and improved the UV resistant properties of composite substrates. [12-14] Chen *et al*. [15] synthesized $TiO_2/BaSO_4$ modified particles with a large surface area using multiple composite growth techniques. After eight composite growths, $TiO_2/BaSO_4$ modified particles with sizes varying from 1.5 to 2.0 μm were formed. The rate of photodegradation of $TiO_2/BaSO_4$ modified particles on methyl orange remained high at 83.5 % even after being used repeatedly for five

*To whom all correspondence should be addressed.

times, demonstrating excellent UV resistance. Therefore, modifying PVC using TiO_2 modified $BaSO_4$ particles improved the dispersion of inorganic fillers in PVC, enhanced the compatibility of inorganic filler powders with PVC, and further promoted the UV resistance, flame-retardant, and mechanical properties of PVC substrates. [16, 17]

In this work, $TiO_2/BaSO_4$ modified particles were prepared using the sol-gel method. Compared to previous studies on $TiO_2/BaSO_4$/PVC composites, the innovation of this work lied in the development of a simpler and more efficient sol-gel route, the systematic optimization of the TiO_2 to $BaSO_4$ ratio (n_{Ti}), and the subsequent achievement of superior particle dispersion and comprehensive performance enhancement in the PVC matrix.

Experimental

Materials

Barium sulfate ($BaSO_4$, ≥ 90 %, CP), were provided by Aoke Powder Co., Ltd. (Shangluo China). Sodium laurylsulfonate (SDS, AR), absolute ethanol (EtOH, AR), ethylene glycol (EG, AR), ammonia (28 %), titanium(IV) oxysulfate-sulfuric acid hydrate ($TiOSO_4 \cdot 2H_2O$, 93 %) and rhodamine B (RhB, GR) were obtained from Aladdin Reagent Co. Ltd. (Shanghai China).

Preparation procedure of $TiOSO_4$/ethylene glycol/H_2O sol

$TiOSO_4 \cdot 2H_2O$ (8.0 g) was dissolved in 50 mL deionized water, left to stand, and filtered to remove insoluble matter or impurities. The pH of the filtrate was adjusted to 7 with ammonia solution. The above titanium oxide sulfate solution, ethylene glycol, and deionized water were mixed uniformly in the ratio of $n_{TiOSO4} : n_{EG}: n_{H2O}$ = (0.5~3):1:4, and stirred (300 rpm) at a constant temperature of 80 ℃ for 30 min to form a homogeneous and transparent titanium sol. The formation of TiO_2 through the sol-gel process involved the following chemical reactions.

$$TiOSO_4 + 2H_2O \rightarrow TiO(OH)_2 + H_2SO_4$$

$$TiO(OH)_2 \rightarrow TiO_2 + H_2O$$

Preparation procedure of $TiO_2/BaSO_4$ particles

$BaSO_4$ (2.0 g) was added to 7 mmol/L SDS solution, dispersed with stirring at 400 rpm at constant temperature at 30 ℃ for 30 min, filtered, washed and dried. The above SDS treated $BaSO_4$ was mixed with $TiOSO_4$/ethylene glycol/H_2O sol, stirred (350 rpm) at a constant temperature in a water bath at 80 ℃ for 1 h, aged at room temperature for 8 h, filtered, washed sequentially with distilled water and EtOH for several times, dried at 105 ℃, and heat treated at 550℃ for 2 h with a heating rate of 10 ℃/min. Finally, TiO_2 modified $BaSO_4$ particles were obtained.

Preparation of $TiO_2/BaSO_4$/PVC composites

According to the ratios shown in Table-1, the above raw materials were mixed in a homogenizing machine for 10 min, and the processing temperature was set at 180 ℃. Then, the mixture was mixed in a double-roller opener for 8 min, hot-pressed and molded in a press at 175 ℃ under a pressure of 10 MPa. The samples were cooled down to room temperature for cutting, and the mechanical properties were tested. The preparation process of $TiO_2/BaSO_4$/PVC composites was schematically illustrated in Fig. 1.

Table-1: Formulation for the preparation of $TiO_2/BaSO_4$/PVC composites.

Composition	PVC	$TiO_2/BaSO_4$	Plasticizer	Thermal stabilizer
Amount/Mass Fraction	100	5-20	20	4

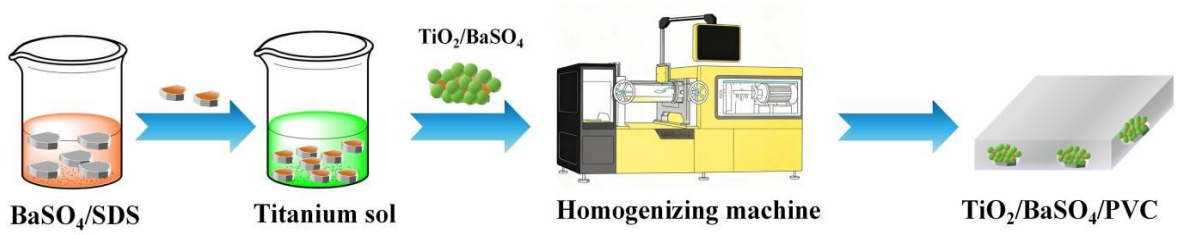

Fig. 1: The schematic of the $TiO_2/BaSO_4$ formation process and interaction with PVC.

Characterization

FTIR spectra of $TiO_2/BaSO_4$ samples were recorded on a Bruker VERTEX V80, 16 scans were accumulated from 400 to 4000 cm^{-1}. The crystal structure of samples were characterized by X-ray diffraction (XRD) using a PANalytical B.V. X'Pert-Powder D/max 2200PC X-ray diffractometer with a Cu Kα (λ=0.1542 nm) anode. The surface morphology of the samples were observed by a HITACHI-S4800 Scanning Electron Microscope (SEM). The samples were coated with Pt. Particle size distribution analysis of $TiO_2/BaSO_4$ was carried out using a Malvern Mastersizer 3000 particle size analyzer.

Determination of settling time and activation degree

$TiO_2/BaSO_4$ (1.0 g) modified particles, were added to a measuring cylinder which contained 50 mL H_2O and dispersed for 1 h. The settling time of each modified sample was recorded.

$TiO_2/BaSO_4$ (0.3 g) modified particles were weighed, dispersed in 60 mL of H_2O, ultrasonic dispersion for 5 min, and then left to stand for 30 min, when the dispersion system no longer changes, the precipitate and the beaker were subjected to constant weight respectively. The activation degree was calculated according to equation (1).

$$X = (1 - \frac{m_2 - m_1}{0.3}) \times 100\% \quad (1)$$

where, X was the activation degree; m_1 was the mass of the beaker after constant weight, g; and m_2 denotes the mass of the precipitate and the beaker after constant weight, g.

Photodegradation performance test of $TiO_2/BaSO_4$/PVC composites

$TiO_2/BaSO_4$/PVC composites was cut into 2 cm×2.5 cm slices and added into 80 mL of 1×10^{-5} mol/L RhB solution, dark adsorbed for 60 min under light-avoidance conditions to reach the adsorption equilibrium, and then the light source was activated to start the degradation experiment. 4 mL supernatant was aspirated from the reaction vial at regular intervals, and the absorbance of the solution was tested using a UV-visible spectrophotometer. The degradation rate was calculated according to equation (2).

$$\eta = \left(1 - \frac{A_0 - A_t}{A_t}\right) \times 100\% \quad (2)$$

where, η was the degradation rate, A_0 was the starting absorbance, and A_t was the absorbance at the moment t.

Flame-retardant property test of $TiO_2/BaSO_4$/PVC composites

The Limit Oxygen Index (LOI) test was an important method for evaluating the flame-retardant property of materials. Referring to GB2406-82 standard for testing, JF-3 oxygen index tester was used. The sample size was 100.0 mm×6.5 mm×3.0 mm, and the permissible deviation was 0.05 mm.

Mechanical properties test of $TiO_2/BaSO_4$/PVC composites

The tensile and peel properties of $TiO_2/BaSO_4$/PVC composites were tested using a universal mechanical testing machine in accordance with GB/T 1040-2006 and GB/T 529-2008 standards, respectively.

Results and discussion

Structural and morphological analysis of $TiO_2/BaSO_4$ composites

Fig 2 displayed the chemical structure of $TiO_2/BaSO_4$ particles with different ratios (n_{TiOSO4} : n_{EG}: n_{H2O} = (0.5~3): 1 : 4). The absorption peaks of SO_4^{2-} were near 638 cm^{-1} and 1128 cm^{-1}. 3400 cm^{-1} was the —OH absorption peak of $BaSO_4$ due to hygroscopicity, and near 1650 cm^{-1} was the H-O-H bending vibration peak. [18] After the formation of $TiO_2/BaSO_4$ composite, a stretch vibrational absorption peak of Ti-O was found near 468 cm^{-1}. [19] Furthermore, the infrared spectra did not reveal any new absorption peaks, suggesting that TiO_2 and $BaSO_4$ were not chemically bonded but rather physically combined. The analytical results indicated that the TiO_2 modified $BaSO_4$ composite materials were successfully prepared by the titanium sol method. The finding of physical combination without chemical bonding was consistent with the work of Wang *et al*. [20], who also reported electrostatic attraction as the primary interaction in $TiO_2/BaSO_4$ systems prepared by co-precipitation. However, the

present sol-gel method achieved comparable composite stability through a simpler and potentially more scalable route.

Structural and morphological analysis of $TiO_2/BaSO_4$ composites

Fig. 2 displayed the chemical structure of $TiO_2/BaSO_4$ particles with different ratios (n_{TiOSO4} : n_{EG}: n_{H2O} = (0.5~3): 1 : 4). The absorption peaks of SO_4^{2-} were near 638 cm^{-1} and 1128 cm^{-1}. 3400 cm^{-1} was the —OH absorption peak of $BaSO_4$ due to hygroscopicity, and near 1650 cm^{-1} was the H-O-H bending vibration peak. [18] After the formation of $TiO_2/BaSO_4$ composite, a stretch vibrational absorption peak of Ti-O was found near 468 cm^{-1}. [19] Furthermore, the infrared spectra did not reveal any new absorption peaks, suggesting that TiO_2 and $BaSO_4$ were not chemically bonded but rather physically combined. The analytical results indicated that the TiO_2 modified $BaSO_4$ composite materials were successfully prepared by the titanium sol method. The finding of physical combination without chemical bonding was consistent with the work of Wang *et al*. [20], who also reported electrostatic attraction as the primary interaction in $TiO_2/BaSO_4$ systems prepared by co-precipitation. However, the present sol-gel method achieved comparable composite stability through a simpler and potentially more scalable route.

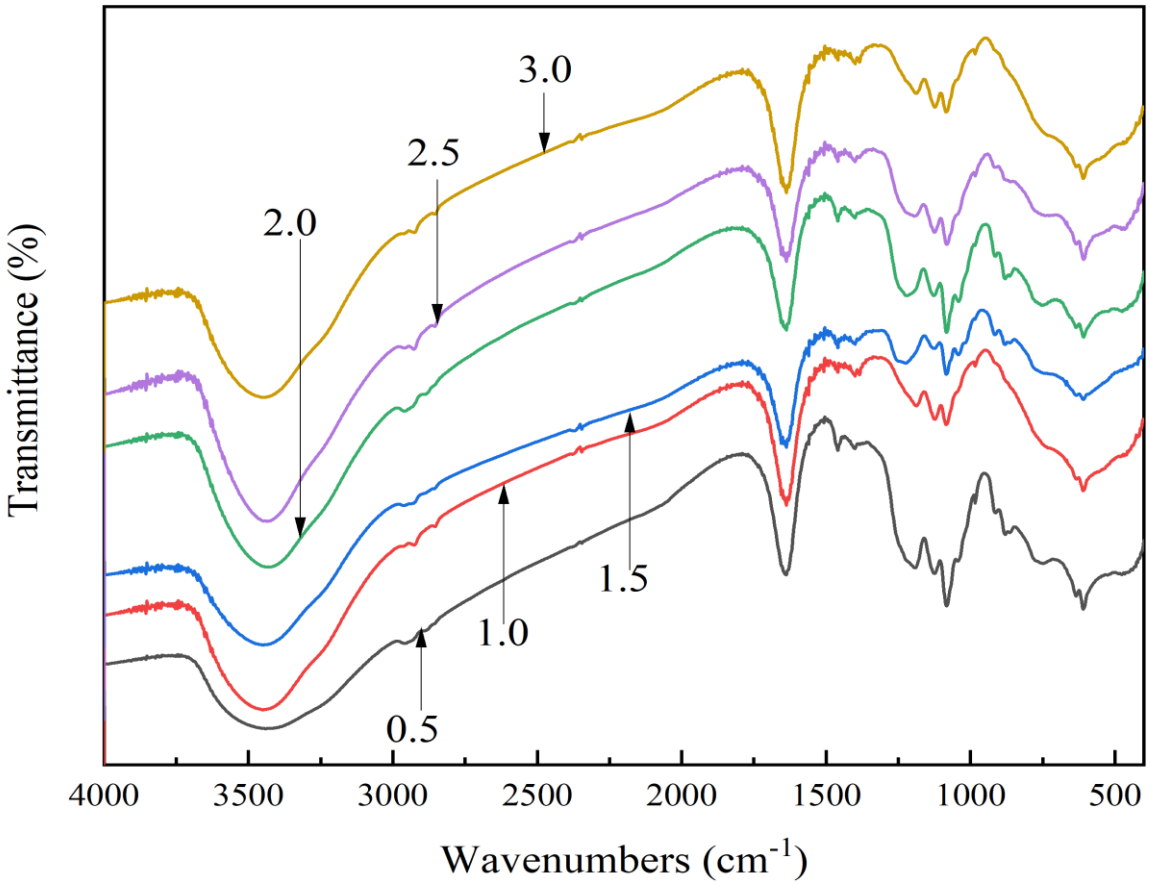

Fig. 2. The FT-IR patterns of $TiO_2/BaSO_4$ particles.

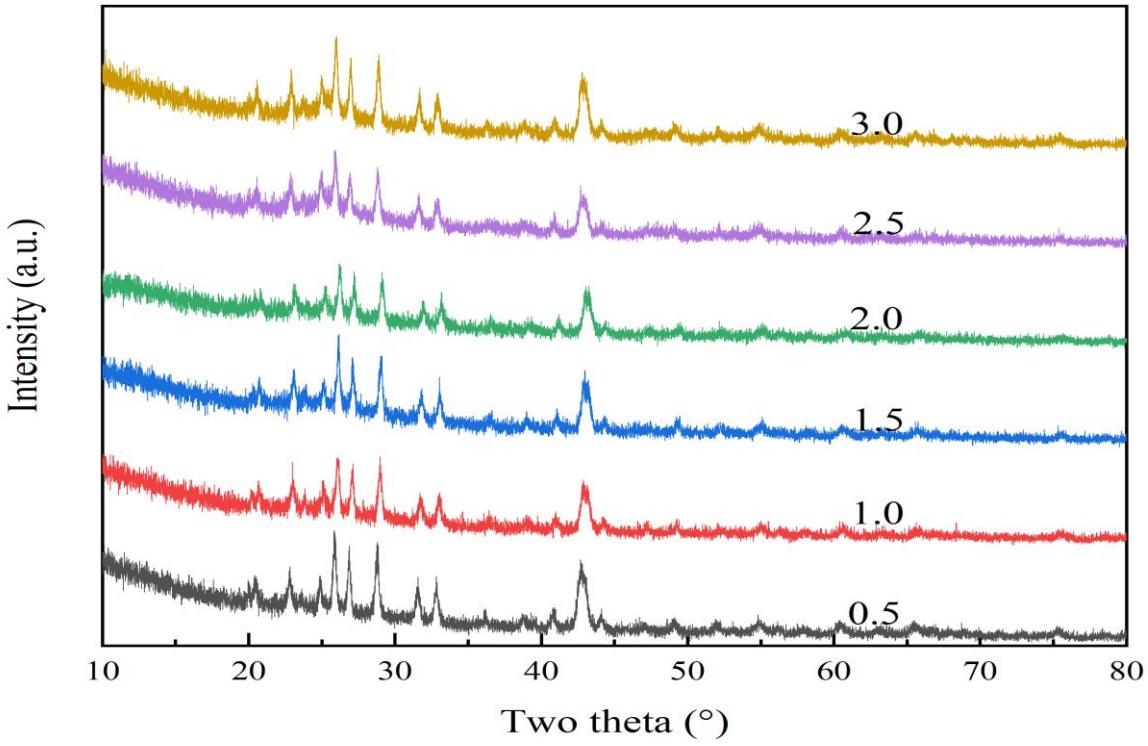

Fig. 3: The XRD curves of $TiO_2/BaSO_4$ particles.

The XRD curves in Fig. 3 revealed the crystalline structure of $TiO_2/BaSO_4$ particles. The diffraction peaks at 2θ = 22.8°, 32.8°, 42.7°, and 49.1° correspond to the 111, 211, 041, and 330 crystal planes of $BaSO_4$. The diffraction peaks of the anatase titanium crystal phase TiO_2 were located at 2θ=25.8° and 54.8°, while the 2θ=36.2° (101) and 40.8° (111) were assigned to the diffraction peaks of the rutile phase TiO_2. [21] The crystalline phase configurations remained unchanged despite varying the TiO_2 content, as illustrated in Fig 4. Incorporating the analytical results of FT-IR, it illustrated that $TiO_2/BaSO_4$ composites could be formed effectively by utilizing the sol-gel method. Furthermore, the comparison of the characteristic diffraction peaks of the modified samples revealed no new crystallization peaks after the formation of $TiO_2/BaSO_4$ materials, indicating that the two materials were mainly bonded by electrostatic gravitational force. Based on the XRD and FT-IR evidence, it was proposed that the primary interaction between TiO_2 and $BaSO_4$ was electrostatic attraction or van der Waals forces, which was consistent with findings reported in previous studies. [20] This physical combination was sufficient to form a stable composite without altering the crystalline phases of the individual components, as confirmed by the XRD patterns.

Fig. 4 displayed the morphology of $TiO_2/BaSO_4$ particles. The $BaSO_4$ composites exhibited an irregular block structure, and the TiO_2 were encapsulated on the surface of $BaSO_4$ in the form of agglomerates. The TiO_2 particles deposited on the $BaSO_4$ surface shown an increasing and decreasing pattern with increasing n_{Ti} contents. When the amount of TiO_2 (n_{Ti}) was between 0.5 and 2.0 mol, the particles deposited on the surface of $BaSO_4$ showed an increasing trend and an obvious agglomeration effect occurred. On the other hand, when the amount of TiO_2 was between 2.5 and 3.0 mol, the deposition of TiO_2 particles on the surface of $BaSO_4$ showed a gradual decrease. When the Ti content was small, hydrogen bonding can form between the active —OH groups on the surface, which effectively improves the interaction with the $BaSO_4$ matrix. [22] As the Ti content gradually increased, the space resistance between the formed TiO_2 particles increased, reducing the surface activity of the composite material and leading to partial detachment of TiO_2 particles.[23]

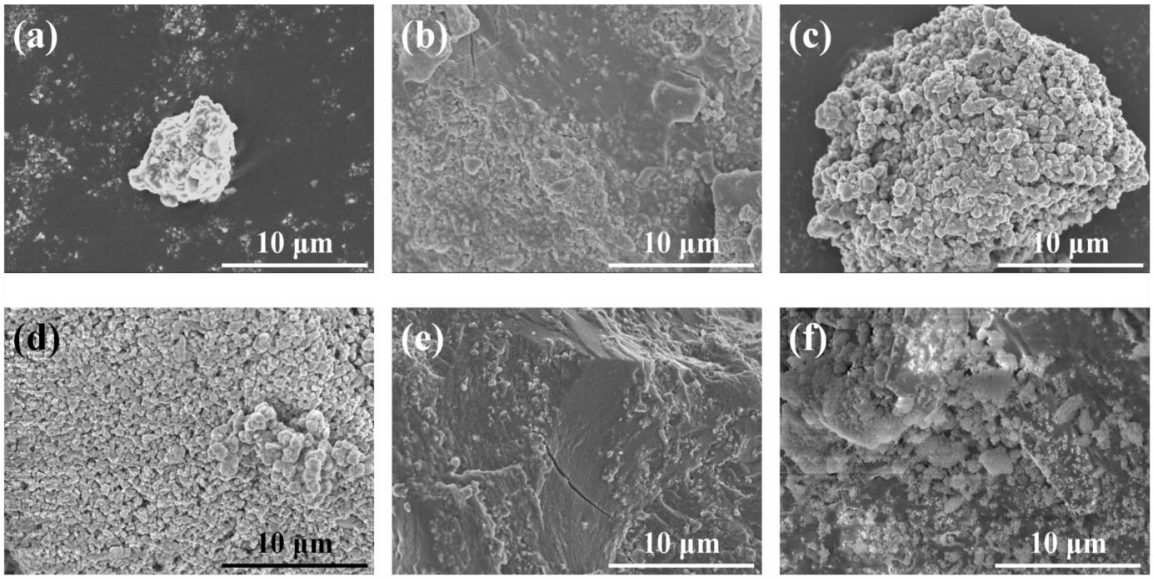

Fig. 4: The SEM morphology of $TiO_2/BaSO_4$ particles: n_{Ti}=0.5 mol (a), n_{Ti}=1.0 mol (b), n_{Ti}=1.5 mol (c), n_{Ti}=2.0 mol (d), n_{Ti}=2.5 mol (e), n_{Ti}=3.0 mol (f).

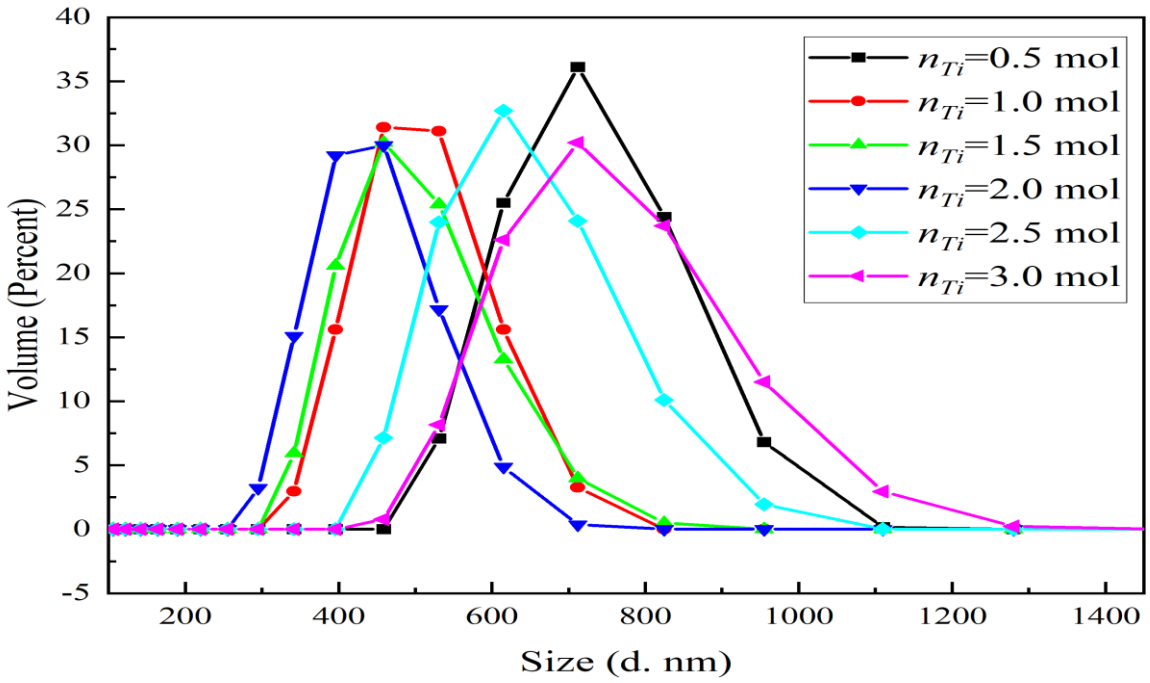

Fig. 5: The particle size distribution curves of $TiO_2/BaSO_4$ particles.

Effect on the particle size distribution of $TiO_2/BaSO_4$ composites

Fig. 5 presented the particle size distribution curves of $TiO_2/BaSO_4$ modified particles. The distribution of particle sizes for $TiO_2/BaSO_4$ particles exhibited a decreasing trend followed by an increasing tendency. When 0.5 mol < n_{Ti} < 2.0 mol, the particle size distribution became broad and inhomogeneous due to agglomeration of the titanium sol formed during hydrolysis. The Ti-O-Ti bonds generated through sol hydrolysis restricted effective

combination with $BaSO_4$, resulting in poor dispersion of the modified materials. When n_{Ti} reached 2.0 mol, the most uniform particle size distribution was achieved, primarily ranging from 256 to 713 nm. This optimized ratio represented a key finding of our composite ratio optimization, which directly led to the improved particle dispersion, as evidenced by the significantly prolonged settling time and enhanced activation degree. When 2.0 mol < n_{Ti} < 3.0 mol, the particle size distribution of $TiO_2/BaSO_4$ particles was wider and non-uniform, the reason was that with the increase of Ti content, the TiO_2 deposited on the surface of $BaSO_4$ becomes difficult to be agglomerated between modified particles due to the spatial potential resistance effect, and with the prolongation of the aging time, the TiO_2 small particles partially regrouped to the surface of barium sulfate. [24]

Effect on settling time and activation degree of $TiO_2/BaSO_4$ composites

The settling time of composites reflected the dispersion effect of the sample. The settling time of the $TiO_2/BaSO_4$ composites exhibited a linear increase, as presented in Fig. 6. The settling time increased with n_{Ti} content, reaching a maximum value of 28.5 h at n_{Ti} = 2.0 mol. This represented an increase of 26.0 h compared to the unmodified sample, indicating significantly improved dispersion stability. Beyond this optimal point, the settling time slightly decreased despite remaining substantially higher than the unmodified reference. This reduction was explained by the increased spatial resistance between TiO_2 particles deposited on the $BaSO_4$ surface at higher n_{Ti} contents, which compromised the dispersion property of $TiO_2/BaSO_4$ composite material.

Activation Degree characterizes the degree to which the $BaSO_4$ material gets modified. As shown in Fig 6, the activation degree of the modified $BaSO_4$ material significantly increases. The maximum activation degree of 82.8 % was achieved at n_{Ti} = 2.0 mol, representing a 49.5 % improvement over unmodified $BaSO_4$. This enhancement resulted from the effective surface coverage of $BaSO_4$ by TiO_2, which transformed the originally polar and hydrophilic surface into a less polar and more hydrophobic one. The improved hydrophobicity prevented sedimentation due to surface tension effects. However, when n_{Ti} exceeded 2.0 mol, the activation degree gradually decreased due to exposure of polar groups caused by TiO_2 agglomeration and insufficient surface coverage, which reduced the hydrophobicity and overall modification efficiency.

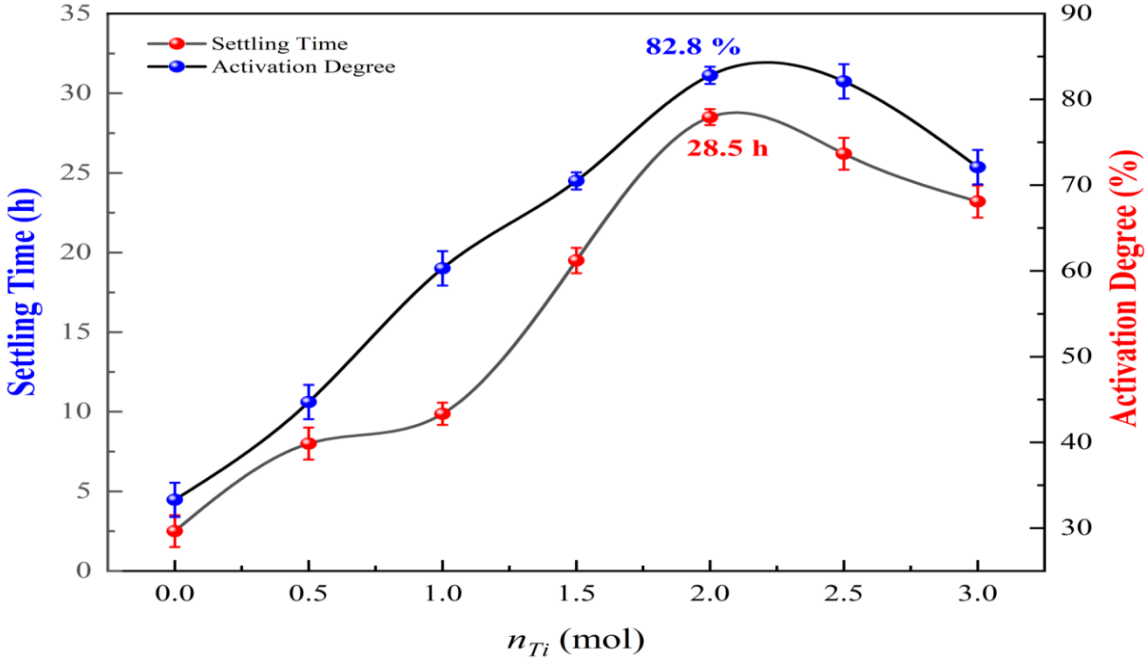

Fig. 6: The settling times and activation degree properties of $TiO_2/BaSO_4$ particles.

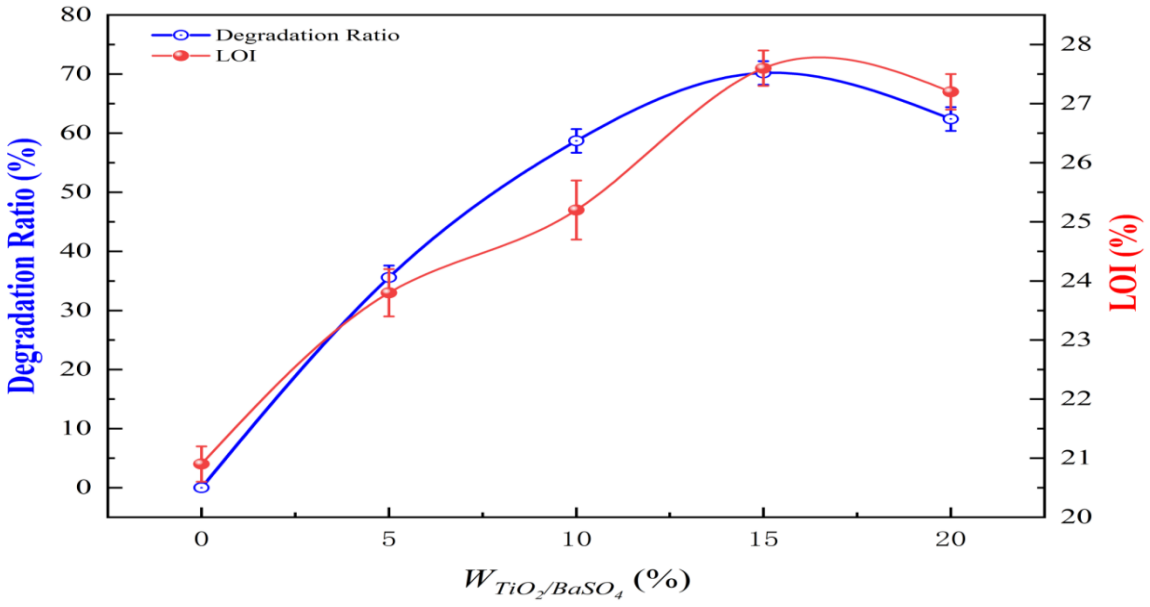

Fig. 7: The RhB photodegradation and LOI properties in $TiO_2/BaSO_4$/PVC composites with different $TiO_2/BaSO_4$ contents.

Photodegradation property and flame-retardant property of $TiO_2/BaSO_4$/PVC composites

The degradation performance of $TiO_2/BaSO_4$/PVC composites on RhB was investigated by varying the mass fraction of $TiO_2/BaSO_4$.. As shown in Fig 7, the RhB degradation efficiency increased gradually with increasing $TiO_2/BaSO_4$ content, reaching a maximum value of 70.2 % at 15 % mass fraction. This degradation efficiency was notably higher than the 58 % RhB degradation reported for pure TiO_2 under similar conditions, [25] indicating a synergistic effect in the $TiO_2/BaSO_4$ composite structure. This superior performance was attributed to the well dispersed $TiO_2/BaSO_4$ particles achieved by the simpler sol-gel route, which provided more active sites and better compatibility with the PVC matrix. However, when the mass fraction exceeded 15 %, particle agglomeration occurred, leading to a reduction in active sites and consequently a decrease in photodegradation efficiency.

The flame-retardant properties of the composites with varying $TiO_2/BaSO_4$ content were also presented in Fig. 7. The Limit Oxygen Index (LOI) initially increased and then decreased with increasing filler content, reaching an optimum LOI value of 27.6 % at 15 % mass fraction. This LOI value compared favorably with other mineral filled PVC systems, such as those incorporating clay or $CaCO_3$, which typically show LOI values below 25 %. [26] The superior flame-retardant was attributed to the formation of a stable and dense carbon layer during thermal degradation, which provided skeleton support for the char formation process and enhanced the barrier effect against heat and oxygen transfer. [26] The $TiO_2/BaSO_4$ composite thus acted as a more effective flame-retardant filler in the PVC matrix, though excessive loading beyond 15 % caused agglomeration and diminished flame-retardant efficiency.

Mechanical properties of $TiO_2/BaSO_4$/PVC composites

The mechanical properties of $TiO_2/BaSO_4$/PVC composites after 150 h of UV irradiation were presented in Fig. 8. As shown in Fig 8a, before UV exposure, the tensile strength decreased with increasing $TiO_2/BaSO_4$ content, which was attributed to interfacial incompatibility and phase defects between the PVC matrix and the composite particles. In contrast, peel strength improved markedly, with the 15 wt% $TiO_2/BaSO_4$ formulation achieving the highest value of 151.52 $N \cdot mm^{-1}$, exceeding that of unmodified PVC by 23.36 $N \cdot mm^{-1}$. This enhancement was consistent with a mechanism in which well dispersed composite particles inhibit crack propagation, thereby increasing the overall toughness of the material.

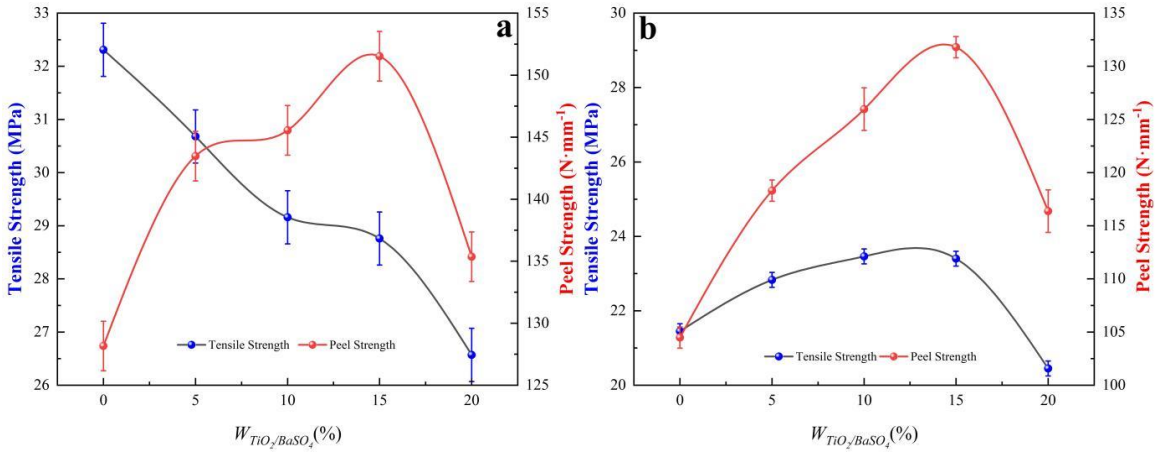

Fig. 8: The mechanical properties of $TiO_2/BaSO_4$/PVC composites: before UV-irradiation (a), after UV-irradiation (b).

After UV irradiation, Fig 8b indicated that pure PVC underwent severe degradation, with reductions in tensile and peel strength of 33.62 % and 18.97 %, respectively. In comparison, the composite containing 15 % $TiO_2/BaSO_4$ exhibited significantly better retention of mechanical properties, with decreases of only 18.64 % in tensile strength and 10.32 % in peel strength. This enhanced UV stability was attributed to the semiconductor nature of the TiO_2 component. When UV photons ($\lambda < 387$ nm) with energy exceeding the bandgap of TiO_2 (3.2 eV) were absorbed, electrons were excited from the valence to the conduction band, generating electron hole pairs. These photogenerated carriers subsequently underwent non-radiative relaxation via electron-phonon coupling, converting the photon energy into lattice vibrational energy. [27] While some radiative recombination occurred at defect sites, thermal conversion remained the dominant energy dissipation pathway. This efficient photothermal mechanism significantly reduced UV penetration into the polymer matrix, thereby suppressing the generation of free radicals such as Cl· and inhibiting chain scission within PVC. [25] The results confirmed that the superior UV resistance stemmed from this fundamental photon energy conversion process.

Conclusion

In conclusion, A $TiO_2/BaSO_4$/PVC composite with enhanced properties was successfully developed. The key innovation of this work was the employment of an optimized and relatively simpler sol-gel method for synthesizing $TiO_2/BaSO_4$ composites, which, through meticulous ratio optimization (n_{Ti} = 2.0 mol), resulted in improved particle dispersion and ultimately superior UV resistance, flame-retardant, and mechanical performance of the PVC composites.

(1) The $TiO_2/BaSO_4$ modified particles were prepared using the sol-gel method. The results indicate that the TiO_2 modified $BaSO_4$ particles have a narrow and uniform particle size distribution (256-713 nm) with n_{Ti} =2.0 mol. The settling time and activation degree of the modified $TiO_2/BaSO_4$ composites reached the maximum values of 28.5 h and 82.8 %, respectively. These values were 26.0 h and 49.5 % higher than the unmodified samples.

(2) The optimal formulation, containing 15 wt% $TiO_2/BaSO_4$ particles, exhibited an LOI of 27.6 % and achieved a RhB photodegradation rate of 70.2 %, representing the highest photodegradation activity among all tested compositions. Mechanical characterization further confirmed the superiority of this composition, which demonstrated a peel strength of 151.52 $N \cdot mm^{-1}$, exceeding that of unmodified PVC by 23.36 $N \cdot mm^{-1}$. Following 150 h of UV irradiation, the composite maintained excellent mechanical integrity, with reductions in tensile and peel strength limited to 18.64 % and 10.32 %, respectively. These findings collectively indicate that the $TiO_2/BaSO_4$/PVC composites offer an optimal balance of photodegradation activity, flame-retardant, and mechanical durability with enhanced UV resistance.

Acknowledgments

We appreciate the financial which support from Doctoral Scientific Research Foundation of Shang Luo University (18SKY003), Science and Technology Innovation Project of the Shaanxi Province Team (2025RS-CXTD-039), Basic Research Program of Natural Science of Shaanxi Province (2019JLM-49).

References

1. M. Ling, D. Ma, X. Hu, Z. Liu, D. Wang, Q. Feng, Hydrothermal treatment of polyvinyl chloride: Reactors, dechlorination chemistry, application, and challenges, *Chemosphere*., **316**, 137718 (2023).
2. A. Al-Muntaser, H M. Abo-Dief, A. E. Tarabiah, E Alzahrani, H. A. Alsalmah, Z. M. Alharbi, R. A. Pashameah, A. Saeed, Incorporated TiO_2 nanoparticles into PVC/PMMA polymer blend for enhancing the optical and electrical/dielectric properties: Hybrid nanocomposite films for flexible optoelectronic devices, *Polym. Eng. Sci.*, **63**, 3684 (2023).
3. S. S. Suresh, S. Mohanty, S. K. Nayak, Preparation of poly (vinyl chloride)/poly (methyl methacrylate) recycled blends: Effect of varied concentration of PVC and PMMA in stability of PVC phase on the recycled blends, *Mater. Today: Proc.*, **5**, 8899 (2018).
4. N. Sen, V. Koli, K. K. Singh, Segmented Microfluidics for Synthesis of $BaSO_4$ Nanoparticles, *Chem. Eng. Process*., **125**, 197 (2018).
5. X. Su, B. L. Shi, Effect of silane coupling agents with different nonhydrolytic groups on tensile modulus of composite PDMS crosslinked membranes, *React. Funct. Polym*., **98**, 1 (2015).
6. J. Li, D. D. Liu, H. Jiang, J. Wang, X. Jing, R. Chen, W. Zhu, S. Han, W. Li, H. Wei, Effects of polyacrylic acid additive on barium sulfate particle morphology, *Mater. Chem. Phys*., **175**, 180 (2016).
7. Y. Li, X. Wang, Y. Cui, W. Ma, H. Guo, High dispersion barium sulfate nanoparticles prepared with dodecyl benzene sulfonic acid, *Int. J. Nanosci*., **11**, 1240040 (2012).
8. A. M. Rabea, M. Mohseni, S. M. Mirabedini, Surface analysis and antigraffiti behavior of a weathered polyurethane-based coating embedded with hydrophobic nano silica, *Appl. Surf. Sci*., **258**, 4391 (2012).
9. J. J. Yang, C. Wang, K. Y. Shao, G. X. Ding, Y. L. Tao, J. B. Zhu, Morphologies, mechanical properties and thermal stability of poly(lactic acid) toughened by precipitated barium sulfate, *Russ. J. Phys. Chem. A*., **89**, 2092 (2015).
10. M. D. Najafi, S. K. Eshkalak, B. Amiri, H. R. Naderi, E. Kowsari, A. Chinnappan, S. Ramakrishna, Green synthesis of fish skeleton-like $BaSO_4$ nanostructures by the ionic liquid designer template as nanofillers for supercapacitors application, *Mater. Today. Chem*., **23**, 100633 (2022).
11. N. Plangpleng, P. Charoenphun, D. Polpanich, Flexible gamma ray shielding based on natural Rubber/$BaSO_4$ nanocomposites, *Radiat. Phys. Chem*., **199**, 110311 (2022).
12. Y. Li, J. Wang, C. Ma, H. Zhang, Preparation and solar-light photocatalytic activity of TiO_2 composites: TiO_2/Kaolin, TiO_2/Diatomite, and TiO_2/zeolite, *Russ. J. Phys. Chem. A*., **88**, 2471 (2014).
13. S. J. Sun, H. Ding, H. Zhou, Preparation of TiO_2-coated barite composite pigments by the hydrophobic aggregation method and their structure and properties, *Sci. Rep*., **7**, 10083 (2017).
14. S. Sun, D. Hao, X. Hou, D. Chen, Y, Chen, Effects of organic modifiers on the properties of TiO_2 -coated $CaCO_3$ composite pigments prepared by the hydrophobic aggregation of particles, *Appl. Surf. Sci*., **456**, 923 (2018).
15. R. Chen, J. Zhou, B. Xu, X. Meng, Preparation of TiO_2/$BaSO_4$ composite microparticles and their photocatalytic activity, *Chem. Eng. J*., **218**, 24 (2013).
16. N. Ahmad, T. Mahmood, Preparation and properties of 4-aminobenzoic acid-modified polyvinyl chloride/titanium dioxide and PVC/TiO_2 based nanocomposites membranes, *Polym. Polym. Compos*., **306**, 35 (2022).
17. N. A. Ramlee, S. S. Mohammad Hanapiah, F. N. Suhaimi, C.T. Ratnam, S. Appadu, Effect of Blend Compositions on Mechanical Properties of Irradiated Titanium Dioxide (TiO_2)/Polyvinyl Chloride (PVC)/Epoxidized Natural Rubber (ENR) Nanocomposites, *Adv. Mater. Res*., **1113**, 43 (2015).
18. T. D. Lam, T. V. Hoang, D. T. Quang, J. S. Kim, Efect of nanosized and surface-modifed precipitated calcium carbonate on properties of $CaCO_3$/polypropylene nanocomposites, *Mater. Sci. Eng. A.*, **501**, 87 (2009).
19. D. Yu, J. Bai, H. Liang, T. Ma, C. Li, AgI-modifed TiO_2 supported by PAN nanofbers: A heterostructured composite with enhanced

visible-light catalytic activity in degrading MO, *Dyes. Pigments.*, **133**, 51 (2016).
20. B. Wang, H. Ding, Y. Wang, Preparation of barite/TiO_2 composite particle and interaction mechanism between TiO_2 and barite particles, *Rare. Metal. Mat. Eng*., **S3**, 193 (2011).
21. N. Nguyen, I. Hwang, T. Kondo, T. Yanagishita, H. Masuda, P. Schmuki, Optimizing TiO_2 nanotube morphology for enhanced photocatalytic H_2 evolution using single-walled and highly ordered TiO_2 nanotubes decorated with dewetted Au nanoparticles, *Electrochem. Commun.*, **79**, 46 (2017).
22. H. Zhou, M. Wang, H. Ding, G. Du, Preparation and characterization of barite/TiO_2 composite particles, *Adv. Mater. Sci. Eng*., **2015**, 878594 (2015).
23. X. Hou, S. Yu, H. Ding, C. Ye, Preparation of sericite-TiO_2 composite particle material by mechano-chemical method and its application, *Adv. Mater. Res*., **427**, 104 (2012).
24. Z. Cao, X. Chen, L. Xing, Y. Liao, M. Xu, X. Li, X. Liu, W. Li, Nano-MnO_2@TiO_2 microspheres: a novel structure and excellent performance as anode of lithium-ion batteries, *J. Power. Sources*., **379**, 174 (2018).
25. Y. Zhang, T. Sun, D. Zhang, Z. Shi, Q. Lin, Enhanced photodegradability of PVC plastics film by codoping nano-graphite and TiO_2, *Polym. Degrad. Stab*., **181**, 109332 (2020).
26. H. F. Pan, W. Wang, Y. Pan, W. R. Zeng, J. Zhang, L. Song, Y. Hu, L. K. Meow, Construction of layer-by-layer assembled chitosan/titanate nanotubes based nanocoating on cotton fabrics: flame retardant performance and combustion behavior, *Cellulose*., **22**, 911 (2015).
27. R. Tejasvi, M. Sharma, K. Upadhyay, Passive Photo-catalytic Destruction of Air-borne VOCs in High Traffic Areas using TiO_2 coated Flexible PVC Sheet, *Chem. Eng. J*., **262**, 875 (2015).